Baroclinic Sea-Level

James C. McWilliams[1], M. Jeroen Molemaker[1], and Pierre Damien[1]

[1]Dept. of Atmospheric and Oceanic Sciences, University of California, Los Angeles, CA 90095

Key Points:

- Sea level, measured relative to a geopotential iso-surface, is the surface dynamic pressure for the oceanic momentum balance.
- Barotropic and baroclinic dynamics combine in determining the sea level.
- Tidal sea level and pressure-gradient force are decomposed into barotropic and baroclinic components in a Pacific Ocean simulation.

Corresponding author: James C. McWilliams, jcm@atmos.ucla.edu

Abstract

Sea level and its horizontal gradient are an expression of oceanic volume, heat content, and currents. Large-scale currents have historically been viewed as mostly "baroclinic", and tides as "barotropic", respectively, in the sense of being strongly related to the oceanic density distribution or not. The purpose of this note is to give dynamical precision to this distinction and, in the particular case of the tides, demonstrate the breadth of their combined barotropic-baroclinic interactions with a realistically forced, high-resolution simulation of the Pacific Ocean circulation. While the different tidal sea-level contributions manifest a horizontal scale separation (*e.g.,* more barotropic at larger scales; more baroclinic surface pressure-gradient force at smaller scales), there are cross-mode corrections in both at the level of tens of percent.

Plain Language Summary

Sea-level variations at tidal frequencies occur because of the "astronomical" gravitational force acting nearly uniformly over the oceanic depth. Thus, they are commonly associated with the depth-averaged velocity, *i.e.,* the barotropic current. However, due to oceanic density stratification and variable bathymetry, the resulting barotropic currents also generate vertically varying (baroclinic) tidal currents that also have an expression in the sea level and surface pressure-gradient force. A prescription is given for how to decompose sea level and its gradient into its barotropic and baroclinic parts, and the answers are illustrated using a Pacific Ocean numerical model.

1 Introduction

Changing sea-level elevation ζ is perhaps the most readily measurable oceanic property. Averaged over surface gravity waves, it expresses the tides and, at lower frequencies, the horizontal pressure gradient force for surface currents $\vec{u}$. At even lower frequencies it expresses climate changes in global temperature and ice volume.

Sea level is traditionally measured with coastal gauges, and in recent decades satellite measurements of elevation and Earth's gravity field have greatly expanded our view.

What is the three-dimensional reality that underlies these surface expressions? To answer this question, measurements are limited and models must be deployed, *i.e.,* geographically and dynamically realistic computational simulations of the oceanic current and density fields.

In the large-scale, low-frequency circulation, ζ is often called the surface dynamic height, and its density-normalized (by ρ_0), horizontal pressure-gradient force is approximately in balance with the local Coriolis force at the surface,

$$-\nabla\phi_s \;=\; -\,g\nabla\zeta \;\approx\; -\,f\,\widehat{\vec{z}}\times\mathbf{u}_{gs}\,. \tag{1}$$

The first equality here is based on hydrostatic balance and the assumption that the air-sea interface is a surface of constant pressure. The surface values are denoted by the subscript s; g is the gravitational constant; f is the Coriolis frequency; $\widehat{\vec{z}}$ is the unit vector in the upward vertical direction; $\mathbf{u}_{gs}$ is the surface geostrophic current; the caret denotes a unit vector; horizontal vectors are bold face; and 3D vectors have an arrow on top. An accompanying vertical momentum relation for the 3D dynamically relevant pressure is hydrostatic balance in an integrated form,

$$\phi(z) \;=\; g\zeta \;-\; \int_z^{\zeta} b\,dz'\,, \tag{2}$$

where the buoyancy field is $b \;=\; g(1 \;-\; \rho/\rho_0)$, ρ is density, and ρ_0 is a constant reference value. In a loose approximation, when only density measurements are available, it

is sometimes assumed that the horizontal pressure-gradient force $\nabla\phi$ vanishes at depth (*i.e.,* below $z = -h_{nm}$, a "level of no motion"), so that the surface dynamic height is entirely due to the interior buoyancy variations b:

$$\zeta^{nm} \approx \frac{1}{g} \int_{-h_{nm}}^{0} b\, dz\,. \tag{3}$$

Here the upper vertical integration limit at $z = \zeta$ has been further approximated by 0, the mean surface elevation (*i.e.,* $\zeta \ll h_{nm}$). While (3) is not fully accurate for basin and mesoscale currents due to its neglect of $\nabla\phi$ at depth, together with (1) it indicates how interior b can influence ζ, hence $\mathbf{u}$. The dynamical influence of b is referred to as baroclinicity, so ζ^{nm} in (3) is a type of baroclinic sea level. However, in this situation of a surface-intensified geostrophic current and no motion at depth, both the barotropic and baroclinic currents defined in (4)-(5) are non-zero; so ζ^{nm} is a mixed barotropic-baroclinic sea level. (See the end of Sec. 2.2 for a further remark.)

For the tides, again $\nabla\phi_s = g\nabla\zeta$ at the relevant frequencies. Tides have an astronomical and self-interaction gravitational forcing that is essentially independent of depth within the ocean. The associated response in $\mathbf{u}$ is the called the "external" tide, which in this paper will be equated with the depth-averaged velocity, a.k.a. the barotropic current, $\mathbf{u}^{bt}$,

$$\mathbf{u}^{bt} = \frac{1}{H+\zeta} \int_{-H}^{\zeta} \mathbf{u}\, dz\,, \tag{4}$$

where $H(\mathbf{x})$ is the resting depth of the ocean. In many papers it is also referred to as the "surface" tide, although that is ambiguous with respect to the barotropic-baroclinic decomposition. The remainder is the "internal" tide, associated with the baroclinic horizontal current,

$$\mathbf{u}^{bc} = \mathbf{u} - \mathbf{u}^{bt}\,, \tag{5}$$

where both $\mathbf{u}$ and $\mathbf{u}^{bc}$ are functions of depth. The existence of an internal tide is evident in interior time series of b, which often show strong oscillations at or near the tidal frequencies. As will be explained in Sec. 2, ζ reflects both barotropic and baroclinic current dynamics.

A simple approximate model for the external tide is to associate the dynamical response to the gravitational forcing with $\mathbf{u}(z) = \mathbf{u}^{bt}$. With an approximation of an incompressible mass balance (*i.e.,* $\vec{\nabla} \cdot \vec{u} = 0$ for 3D $\vec{u}$, because ρ variations are small compared to ρ_0) and the kinematic boundary conditions at the solid bottom and top free surface, the column-integrated continuity relation is

$$\partial_t \zeta = -\nabla \cdot \big((H+\zeta)\mathbf{u}^{bt} \big)\,. \tag{6}$$

Integrated over the area of the domain, this relation implies that the ocean has a constant volume (ignoring rivers and other surface freshwater volume fluxes, all of which have small effects on tidal time scales). Notice that (6) has no explicit dependency on b. With a further approximation that $b = 0$, (2) implies that $\nabla\phi(z) = \nabla\phi_s = g\nabla\zeta$, and a horizontal momentum balance can be formulated entirely in terms of $\mathbf{u}^{bt}$, which together with (6) is called the Shallow-Water Equations. It can also be called a barotropic tidal model with $\zeta = \zeta^{bt}$. One of the first satellite tidal products was G. Egbert et al. (1994) that fits a Shallow-Water model to altimetric measurements. This model is dynamically inconsistent with (2) as it neglects any baroclinic effect from $b \neq 0$, and it is quite different from (3); nevertheless, it has been widely considered useful as an estimate of ζ at large spatial scales comparable to the width of oceanic basins, associating it with the barotropic tide. A model of the barotropic tide by itself is dynamically incomplete, and any such model, with whatever mixture of dynamics and measurements, has to confront the important matter of energy conversion to the baroclinic tide that occurs in stratified waters over variable topography (Stammer et al., 2014).

From the perspective of this paper, a sufficiently accurate model for tides and other currents is the Boussinesq, hydrostatic, incompressible (*i.e.,* non-divergent $\vec{u}$) equations that also contain a realistic seawater equation of state and necessary forcing and damping effects. In this system, (2) and (4)-(6) are correct relations, while (1) and (3) are only approximations for the indicated circumstances. The specific question posed here is how the sea level should be partitioned into barotropic and baroclinic components and, more specifically, how the astronomically forced external and internal tides should be partitioned dynamically. The theoretical answer is illustrated with Pacific-basin simulations using the Regional Oceanic Modeling System (ROMS) (Shchepetkin & McWilliams, 2005) that embodies the dynamical assumptions listed in this paragraph.

2 Baroclinic-barotropic decomposition

2.1 Background

Multiple approaches have been taken for determining the barotropic-baroclinic decomposition of the tides. The direct approach of evaluating (4)-(5) is rarely available from measurements of the full water column, and it would not directly show the decomposition of sea level.

One approach to the decomposition

$$\zeta \;=\; \zeta^{bt} \,+\, \zeta^{bc} \tag{7}$$

is by Colosi and Munk (2006), who analyzed very long time series of $\zeta(t)$ at two tide gauges in Hawaii. They devised a statistical model for the shape of the frequency spectrum that assumed that the barotropic component is entirely a "coherent" spectrum line (*i.e.,* in phase with the astronomical forcing, a.k.a. the equilibrium tide), while the baroclinic component has both a coherent line and a smoothly varying "incoherent" shape in nearby frequencies in association with refraction caused by spatial variations in subtidal b; the latter split is measured by the variance in the phase at the tidal frequency. They concluded that for the M_2 frequency ζ^{bt} is much larger than ζ^{bc}, while the latter has comparable magnitudes in its coherent and incoherent parts. This is an adynamical analysis. It also has no information about $-\,g\nabla\zeta$, which is the horizontal pressure-gradient force.

Savage et al. (2017) analyze a realistic global simulation model (HYCOM) and define a "steric" sea-level anomaly by

$$\zeta^{st} \;=\; \frac{1}{g}\int_{-H}^{\zeta} b\,dz\,. \tag{8}$$

They then associate ζ^{st} with ζ^{bc} and define a "non-steric" (barotropic) residual, $\zeta^{bt} = \zeta - \zeta^{bc}$. Their conclusions regarding the tidal sea-level decomposition are qualitatively consistent with those of Colosi and Munk (2006) and have the advantage of global coverage. Notice the functional similarity between (8) and the low-frequency approximation ζ^{nm} in (3), apart from a difference of integration range. In our view this definition, while motivated by a conception of seawater compressibility, is not dynamically defensible, as further explained in Sec. 2.2.

Kelly (2016) opens with "The *de facto* standard is to define surface tides as depth-averaged pressure and horizontal velocity and internal tides as the residuals", which we almost agree with. He then proceeds, as his main topic, to define vertical modes, associating mode 0 with the barotropic mode and modes 1, 2, ... with the baroclinic modes. Part of his paper is to include a correct free-surface boundary condition in the modal calculation, even though that introduces a modest discrepancy with the principle quoted here. (With a rigid-lid boundary condition, it does conform; see Appendix.) Thus, the

linear, conservative, free-surface, gravest (a.k.a. "barotropic") eigenmode $\mathbf{u}_o$ for they hydrostatic Primitive or Boussinesq equations does not exactly coincide with the depth-averaged $\mathbf{u}^{bt}$ defined here in (4), and the depth-average of the " baroclinic" eigenmodes, $\mathbf{u}_n$, $n \geq 1$, are not exactly zero, again in contrast with $\mathbf{u}^{bc}$ here, although these eigenmodes nearly have these depth-averaged attributes and their differences with rigid-lid eigenmodes, with these exact attributes, is slight. However, this difference does allow the $\mathbf{u}_0$ eigenmode to escape the discrepancy of non-zero ζ_0 while still satisfying the continuity equation (6).

In general we find vertical modes somewhat problematic as a representation for realistic situations because they presume as background the local values of resting depth H and sub-tidal stratification profile $N^2(z) = db/dz$, both of which are geographically variable (temporally, too, for N^2). However, our primary criticism is that this principle does not give a dynamically correct decomposition of the horizontal pressure-gradient force for general $b(\mathbf{x})$ and $H(\mathbf{x})$, as further explained in Sec. 2.2.

In practice the most common approach for decomposing tidal ζ, both for satellite measurements and models, is on the basis of horizontal scale content (Carrere et al., 2021; Ubelmann et al., 2022). The conservative, linear eigenmodes for a flat, resting ocean at the tidal frequencies — whose vertical structure is consistent with Kelly (2016) — have a very large horizontal wavelength of $O(10^4)$ km for the barotropic mode, in contrast with $O(10^2)$ km for the baroclinic modes, which are near the baroclinic deformation radius $\sim Nh_{pyc}/f$, where h_{pyc} is the depth of the main pycnocline. Of course, real tidal dynamics are forced and damped, if not also nonlinear, but this criterion does provide a heuristically plausible framework for the decomposition. However, it too is dynamically flawed due to coupling between barotropic and baroclinic currents (Secs. 2.2 and 3.2).

Thus, we conclude that none of the existing approaches for making a barotropic-baroclinic tidal decomposition is fundamentally well-grounded, even though many of these approaches have come to sensible and mutually consistent conclusions about the physical characteristics of the tides.

2.2 Dynamical decomposition

The fundamental basis for a barotropic-baroclinic decomposition in a model like ROMS is in terms of the horizontal velocity $\mathbf{u}$, *i.e.,* (4) and (5). While (6) suggests that sea level is associated with the barotropic velocity, the evolution equation for the latter cannot be closed entirely in terms of the sea level as its pressure-gradient force. Rather, the barotropic horizontal momentum equation has the form of

$$\partial_t \mathbf{u}^{bt} \;=\; -\,\frac{1}{H+\zeta}\int_{-H}^{\zeta} \nabla\phi\, dz' \;+\; \ldots \;\equiv\; \mathbf{P}^{bt} \;+\; \ldots\,, \tag{9}$$

with a depth-averaged pressure-gradient force $\mathbf{P}^{bt}$; the dots indicate the non-pressure forces elided here (Shchepetkin & McWilliams, 2005). Using (2), we can evaluate this barotropic force to be

$$\mathbf{P}^{bt} \;=\; -\,g\nabla\zeta \;-\; \mathbf{P}^{bc}(\zeta)\,, \tag{10}$$

and the corresponding vertical profile of the baroclinic pressure-gradient force is

$$\mathbf{P}^{bc}(z) \;=\; \nabla\int_{z}^{\zeta} b\, dz' \;-\; \frac{1}{H+\zeta}\int_{-H}^{\zeta} \nabla\left(\int_{z'}^{\zeta} b\, dz''\right) dz'\,, \tag{11}$$

with a surface value of

$$\mathbf{P}^{bc}(\zeta) \;=\; -\,\frac{1}{H+\zeta}\int_{-H}^{\zeta} \nabla\left(\int_{z'}^{\zeta} b\, dz''\right) dz'\,. \tag{12}$$

Thus, the total surface pressure-gradient force is, as expected,

$$\mathbf{P}^{bt} + \mathbf{P}^{bc}(\zeta) = -g\nabla\zeta\,. \tag{13}$$

The relations (9)-(13) make it clear that the evolution of the barotropic current is influenced by the buoyancy field as well as the sea level; *i.e.,* the barotropic and baroclinic currents have a coupled dynamics in a stratified ocean, and ζ and $\mathbf{P}$ cannot be uniquely associated with either one alone, as in (7) and (13).

To make the coupling explicit, ζ changes due to a divergence in the barotropic transport, $\mathbf{u}^{bt}$ changes due to the depth-averaged pressure-gradient force involving both ζ and b, and this then feeds back onto further ζ changes; meanwhile b changes due to both $\mathbf{u}^{bt}$ and $\mathbf{u}^{bc}$. Only for the rigid-lid linear normal modes (Sec. 2.1 and Appendix) is this barotropic-baroclinic coupling broken with our definition of $\mathbf{u}^{bt}$.

The governing momentum equations contain a pressure-gradient force, not the pressure *per se*. With the Boussinesq approximation where $|b| \ll g$ and in deep water where $|\zeta| \ll H$, these two expressions for $\mathbf{P}^{bc}$ can be simplified by setting $\zeta \approx 0$. However, for variable $H(\mathbf{x})$, $\mathbf{P}^{bc}$ cannot be expressed in the form of a baroclinic sea-level gradient, because ∇ does not commute with H; hence, we cannot identify a ζ^{bc} such that $\mathbf{P}^{bc}(\zeta) = -g\nabla\zeta^{bc}$.

If we manipulate (12), we can write

$$\mathbf{P}^{bc}(\zeta) = -g\nabla\widetilde{\zeta}^{bc} + \mathbf{R}^{bc} \tag{14}$$

with a baroclinic pseudo sea-level,

$$\widetilde{\zeta}^{bc} = \frac{1}{g(H+\zeta)} \int_{-H}^{\zeta} \left(\int_{z'}^{\zeta} b\, dz'' \right) dz'\,, \tag{15}$$

and a residual contribution to the baroclinic pressure-gradient force,

$$\mathbf{R}^{bc} = \frac{1}{H+\zeta} \int_{-H}^{\zeta} \left(b\nabla H - \frac{1}{H+\zeta} \left(\int_{z'}^{\zeta} b\, dz'' \right) \nabla(H+\zeta) \right) dz'\,, \tag{16}$$

that is associated with resting-depth gradients. Again, one can simplify these expressions with $\zeta \approx 0$. Notice that $\widetilde{\zeta}^{bc}$ in (15) differs from ζ^{st} in (8) by an extra vertical integral associated with the vertical averaging in the barotropic momentum equation.

In fact, $\widetilde{\zeta}^{bc}$ is equivalent to minus the buoyancy contribution to the depth-averaged pressure from (2); *i.e.,*

$$\frac{1}{H+\zeta} \int_{-H}^{\zeta} \phi(z')\, dz' = g\,(\zeta - \widetilde{\zeta}^{bc})\,, \tag{17}$$

which itself is equal to g times the barotropic pseudo sea-level $\widetilde{\zeta}^{bt}$. The existence of $\mathbf{R}^{bc} \neq 0$ in (14) shows that the depth-averaged pressure gradient differs from the gradient of the depth-averaged pressure.

Notice that $\mathbf{R}^{bc}$ vanishes for a flat bottom, whence with this ζ simplification,

$$\mathbf{P}^{bc} = -g\nabla\widetilde{\zeta}^{bc} \qquad \text{and} \qquad \widetilde{\zeta}^{bc} \approx \frac{1}{gH} \int_{-H}^{0} \left(\int_{z'}^{0} b\, dz'' \right) dz'\,, \tag{18}$$

when $\nabla H = 0$. This partition in (14) is intended only to demonstrate the $\widetilde{\zeta}^{bc}$ component. In particular, note that the unpartitioned $\mathbf{P}^{bc}(\zeta)$ in (12) does not have any direct dependency on ∇H; rather, that arises only in the partitioned expressions. For linear eigenmodes over a flat bottom, $\zeta^{bt} \approx \zeta$ and $\widetilde{\zeta}^{bc}$ is small for the barotropic mode, and *vice versa* for the baroclinic modes. The baroclinic pseudo sea level $\widetilde{\zeta}^{bc}$ has a partial similarity with the steric ζ^{st} in (8).

Thus, we propose a dynamical decomposition of the horizontal pressure-gradient force (10)-(13) based on the barotropic-baroclinic decomposition of $\mathbf{u}$, rather than a direct decomposition of sea level itself except where H is flat. The baroclinic contribution (*e.g.,* $\widetilde{\zeta}^{bc}$ in (18)) can be compared with the baroclinic expressions for ζ^{nm} in (3) and for ζ^{st} in (8); it has similar ingredients but it adds another vertical integral. With most $b(z)$ profiles the different ζ values will be quantitatively different but similar in magnitude.

This decomposition is valid for all frequencies. The application to tides is perhaps the most timely one with the prospect of new altimetric satellites with higher spatial resolution. To make this focus, the expressions in this section should be temporally filtered to isolate the tidal frequencies. With the simplification $|\zeta| \ll H$, these expressions are linear in ζ and b, which makes the filtering task easier. Furthermore, the decomposition does not depend on calculating vertical modes (Kelly, 2016), although that is a further analysis option. And, it makes no assumption *a priori* about the spatial scale content of the barotropic and baroclinic components. For the special case of conservative linear, rigid-lid, tidal eigenmodes, the Appendix shows that the relations in this section yield the familiar modal results.

Finally, in the low-frequency context of many upper-ocean currents where ζ^{nm} is relevant (Sec. 1), $\zeta = \zeta^{nm}$, and $\zeta^{bt} = \zeta^{nm} - \widetilde{\zeta}^{bc}$, where $\widetilde{\zeta}^{bc}$ has the same sign as but is smaller in magnitude than ζ^{nm}. Thus, ζ^{bt} is reduced (*i.e.,* partly "compensated") compared to ζ, and the vertical isopycnal displacements in the interior, $\eta \approx -b/N^2$, have the opposite sign as the sea level ζ. $\mathbf{u}^{bt}$ and $\mathbf{u}^{bc}$ have the same sign in the upper ocean and approximately cancel at depth. (This is not the tidal situation.)

The choice here for the dynamically relevant decomposition of the surface pressure-gradient force has some similarity with the long-standing discussion about the role of bathymetry in large-scale circulation. Several alternative interpretive frameworks have been adopted, all correct and variously helpful for physical understanding: the vertical curl of the depth-averaged horizontal momentum balance (*i.e.,* the barotropic balance), featuring the Joint Effect of Baroclinicity and Relief (JEBAR) (Sarkisyan & Ivanov, 1971; Mellor, 1999); the curl of the depth-integrated momentum balance (*i.e.,* the transport balance), featuring the Bottom Pressure Torque (BPT) (Song & Wright, 1998; M. J. Molemaker et al., 2015); and the depth-integral of the curl of the momentum balance (*i.e.,* the vorticity balance), featuring the Bottom Stress Divergence Torque (BSDT) (Jagannathan et al., 2021; Capo et al., 2023). These alternatives arise from the non-commutivity of the vertical integral or average and the horizontal gradient of H, as in (14)-(16). For the tides the vorticity or circulation tendency is less relevant than the force, hence the focus there is on the pressure-gradient force, using the depth-averaged decomposition in (9)-(13).

3 Illustration

3.1 Pacific simulation

The UCLA version of ROMS (the Regional Oceanic Modeling System; Shchepetkin and McWilliams (2003, 2005)) is a terrain-following oceanic circulation model. It uses third-order upwind advection algorithms for the horizontal advection of tracers and momenta. These advection schemes have a dissipative discretization error that is hyper-diffusive or -viscous in nature and automatically scales with resolution, negating the need for an explicitly prescribed horizontal smoothing or regularization term. Vertical advection is computed with a fourth-order spline advection scheme. Unresolved mixing processes are parameterized with a the K-profile parameterization in the surface and bottom boundary layers, combined with a Richardson number based parameterization in the interior (Large et al., 1994).

The simulation that is the foundation of the investigation in this paper is a basin-scale simulation of the full Pacific Ocean with a nominal horizontal grid resolution of $dx =$ 6 km. It is a high-resolution descendant of the well-validated simulation in Lemarié et al. (2012) with additional tidal forcing. Strictly speaking, this is still a regional simulation that needs to be forced at its lateral boundaries, which are most extensive in the south. The information for these open boundaries is derived from the GLORYS reanalysis data set (Verezemskaya et al., 2021) that is provided at at resolution of 0.083 degree and a time interval of 1 day. The GLORYS data are interpolated in space to the computational grid and interpolated in time at each time-step while the model is running. We refer to these type of computations as 'online' computations. This is in contrast with pre- and post-processing of data before or after the model run, which we refer to as 'offline' computations. The GLORYS data does not contain tidal information, and the basin-scale simulation is tidally forced at the open boundaries with sea-surface elevations and tidal barotropic currents from the TPXO9 analysis (G. D. Egbert & Erofeeva, 2002). In addition to this tidal forcing at the lateral boundaries, the model is forced with a surface geopotential forcing. The surface geopotential is a combination of the astronomical tide and the self-attraction and loading effect (Arbic et al., 2018). The self attraction and loading are the result of geopotential anomalies that arise from the evolving sea surface elevation itself as well as the deformation of Earth's crust under the influence of the tidal motions (Arbic et al., 2018). Atmospheric forcing is obtained from the ERA5 global reanalysis (Hersbach et al., 2020). This dataset is available at a nominal 0.25 degree spatial resolution and hourly intervals. The COARE formulation (Fairall et al., 2011) is used to compute momentum and tracer fluxes from atmospheric variables using a bulk approach. The use of sufficiently high-frequency atmospheric forcing permits realistic levels of near inertial internal waves below the mixed layer, which are essential to a correct representation of the kinetic energy budget in the ocean (Shcherbina et al., 2013; Barkan et al., 2021). A more complete description of the tidal simulation and its analyses are in separate papers (M. Molemaker, Damien, Dauhajre, & McWilliams, 2023; M. Molemaker, Damien, McWilliams, et al., 2023).

3.2 Tidal pressure-gradient force

We now focus on the tidal components of the Pacific simulation, and even more particularly on the lunar semi-diurnal (M2) component that on average has the largest amplitude among the components. They are extracted by time filtering the model output at this frequency of 2.237×10^{-5} cycles per second. The M2 signal is defined as the complex Fourier amplitude of a single frequency in this time series whose length is an integer multiple of its period. Eight months of model output data are analyzed here, which is sufficient to accurately extract the M2 signal with its 466 cycles.

The purpose of this paper is to decompose the surface pressure-gradient force, $-g\nabla\zeta$, into its barotropic and baroclinic components. Furthermore, using the approximation (15), we can even decompose the sea-level ζ itself, noting *a postiori* that the "integral" of $\mathbf{R}^{bc}$ in (16) is rather small on larger scales, even compared to $\widetilde{\zeta}^{bc}$ itself, where integral here is defined as the solution for a surface potential field Z that satisfies the Poisson equation,

$$\nabla^2 Z = \frac{1}{g}\nabla\cdot\mathbf{R}^{bc}\,, \tag{19}$$

with zero Neumann boundary conditions; more is said about about $\mathbf{R}^{bc}$ near the end of this section.

The sea-level decomposition is shown in Fig. 1. In these plots only a single phase in the M2 cycle is shown, but it is representative of the scales and patterns of the tide throughout its cycle. As expected, the ζ field appears smooth on the basin scale, and it is visually similar to the barotropic pseudo sea-level $\widetilde{\zeta}^{bt}$; however, their difference, $\widetilde{\zeta}^{bc}$ is not particularly small (*i.e.,* about 20% in amplitude), and this difference represents

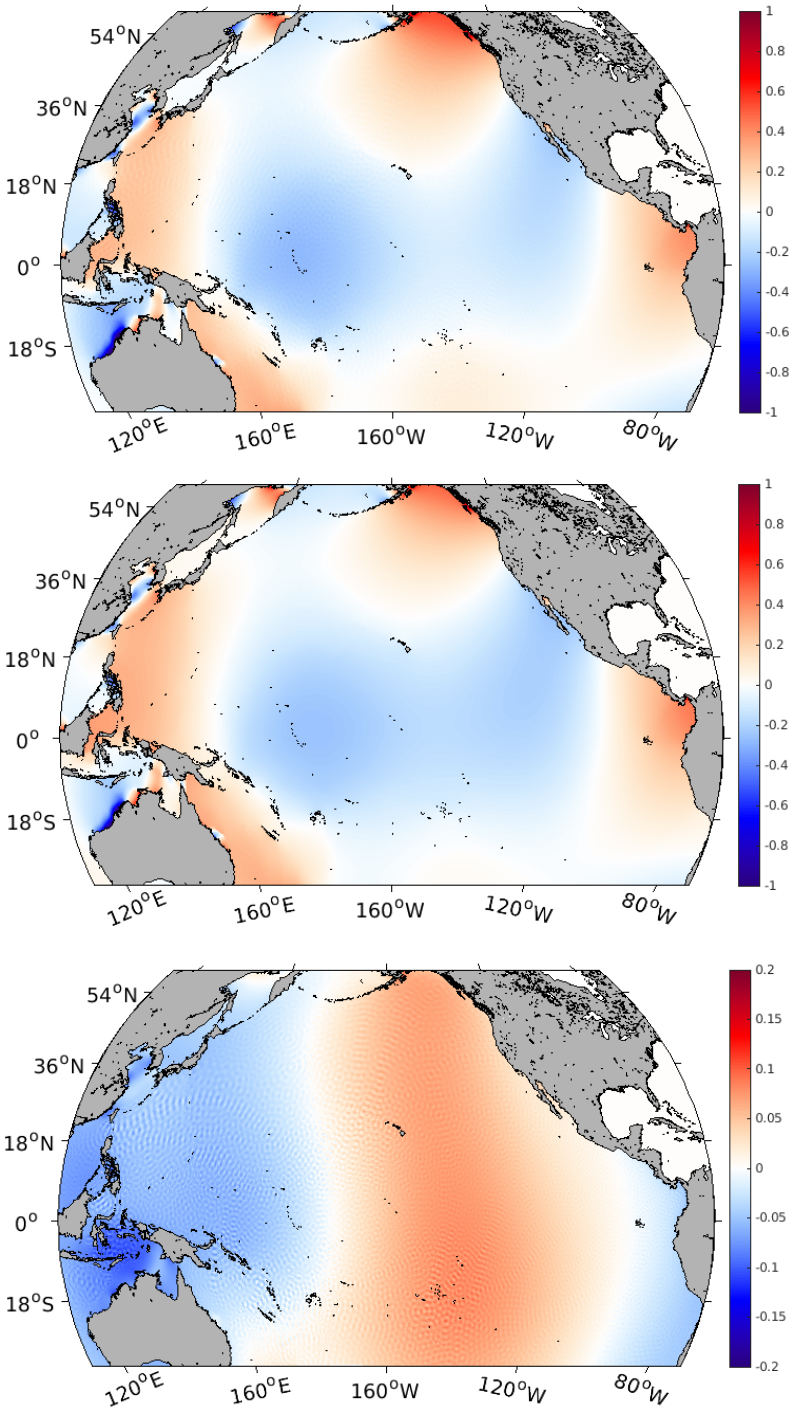

Figure 1. (top) Sea-level ζ [m], (middle) barotropic pseudo sea-level $\widetilde{\zeta}^{bt} = \zeta - \widetilde{\zeta}^{bc}$ [m], and (bottom) baroclinic pseudo sea-level $\widetilde{\zeta}^{bc}$ [m] for a single phase of the M2 tide in the Pacific Ocean. Note the reduced colorbar range for $\widetilde{\zeta}^{bc}$ and the more evident small-scale fluctuations.

the dynamical inconsistency in modeling the barotropic tide without including the buoyancy variations that represent the dynamical influence of modal coupling. The basin-scale pattern of $\widetilde{\zeta}^{bc}$ is quite different from that of $\widetilde{\zeta}^{bt}$; thus, there is little evidence of "compensation" between these components (*cf.,* ζ^{nm}). Furthermore, in $\widetilde{\zeta}^{bc}$ the smaller scale structure is more visually evident as "ripples" at approximately the mesoscale baroclinic deformation radius length of $O(100)$ km, especially in the western Pacific, where the baroclinic tidal amplitude is very strong, but also around other islands and ridges in the central and equatorial Pacific.

The analogous surface pressure-gradient forces are in Fig. 2 with averaging over the M2 tidal cycle. Now the interior patterns are dominated by mesoscale structures that are quite inhomogeneously related to island and topographic generation sites, again as expected from baroclinic tidal generation by energy conversion from the astronomically forced tides at those sites. Many of the edge patterns are associated with shallow shelves and coasts where the barotropic tide is both amplified and dissipated. Most of the interior mesoscale patterns are mostly associated with $\mathbf{P}^{bc}$, *i.e.,* the baroclinic tide, but there are locations where $\mathbf{P}^{bt}$ is not small, *e.g.,* especially near undersea ridges. Its interior magnitude can be nearly half of that of $\mathbf{P}^{bc}$. The importance of $\mathbf{P}^{bt}$ in broad regions indicates that there is persistent barotropic-baroclinic dynamical coupling even away from the topographic generation sites for the internal tide. The common practice of interpreting mesoscale tidal signals in $\nabla\zeta$ as entirely baroclinic, mostly based on the linear eigenmode decomposition (Sec. 2.1 and Appendix), is a fairly good approximation, but not a perfect one because $\mathbf{P}^{bt}$ is not uniformly smaller than $\mathbf{P}^{bc}$.

A further decomposition of the barotropic pressure gradient force $\mathbf{P}^{bt}$ is shown in Fig. 3). It shows that the part of the force associated with the depth-averaged pressure,

$$\begin{aligned} -g\,(\zeta-\widetilde{\zeta}^{bc} &= -\frac{1}{H+\zeta}\int_{-H}^{\zeta} dz'\,\left(g\zeta - \int_{z'}^{\zeta} dz'' b\right) \\ &= -g\zeta + \frac{1}{H+\zeta}\int_{-H}^{\zeta} dz' \int_{z'}^{\zeta} dz'' b\,, \end{aligned} \tag{20}$$

is almost everywhere larger than the part due to interactions between the pressure and topographic gradient, $\mathbf{R}^{bc}$ in (16). The exceptions are near the island and ridge lines where ∇H is large. Thus, for many purposes, $\widetilde{\zeta}^{bc}$ can be viewed as the baroclinic sea level field.

These figures demonstrate that there is important dynamical coupling between the barotropic and baroclinic tides throughout most of the domain, beyond the particular topographic locations where baroclinic generation occurs. A fuller and more phenomenological interpretation of the heterogeneous tidal signals, especially for the complex spatial patterns in $\mathbf{P}^{bc}$ and $g\nabla\zeta$ (Fig. 2), is made in M. Molemaker, Damien, Dauhajre, and McWilliams (2023).

4 Summary and Conclusions

A dynamically consistent barotropic-baroclinic decomposition of the pressure-gradient force is based on the definition of the barotropic horizontal velocity as the depth-averaged current. This implies there is a significant buoyancy influence on the (depth-averaged) pressure-gradient force for the barotropic current.

At the surface this force cannot be decomposed into sea-level gradients because of variations of oceanic depth. The barotropic force has a contribution from the double depth integral of the density field in (10) (but not simply the steric sea level ζ^{st} in (8)), as well as the familiar - $g\nabla\zeta$ force.

At basin scales the tidal ζ is mostly barotropic, and at mesoscales the surface pressure gradient $-g\nabla\zeta$ is mostly due to - $\mathbf{P}^{bc}$. While this approximate scale partition can

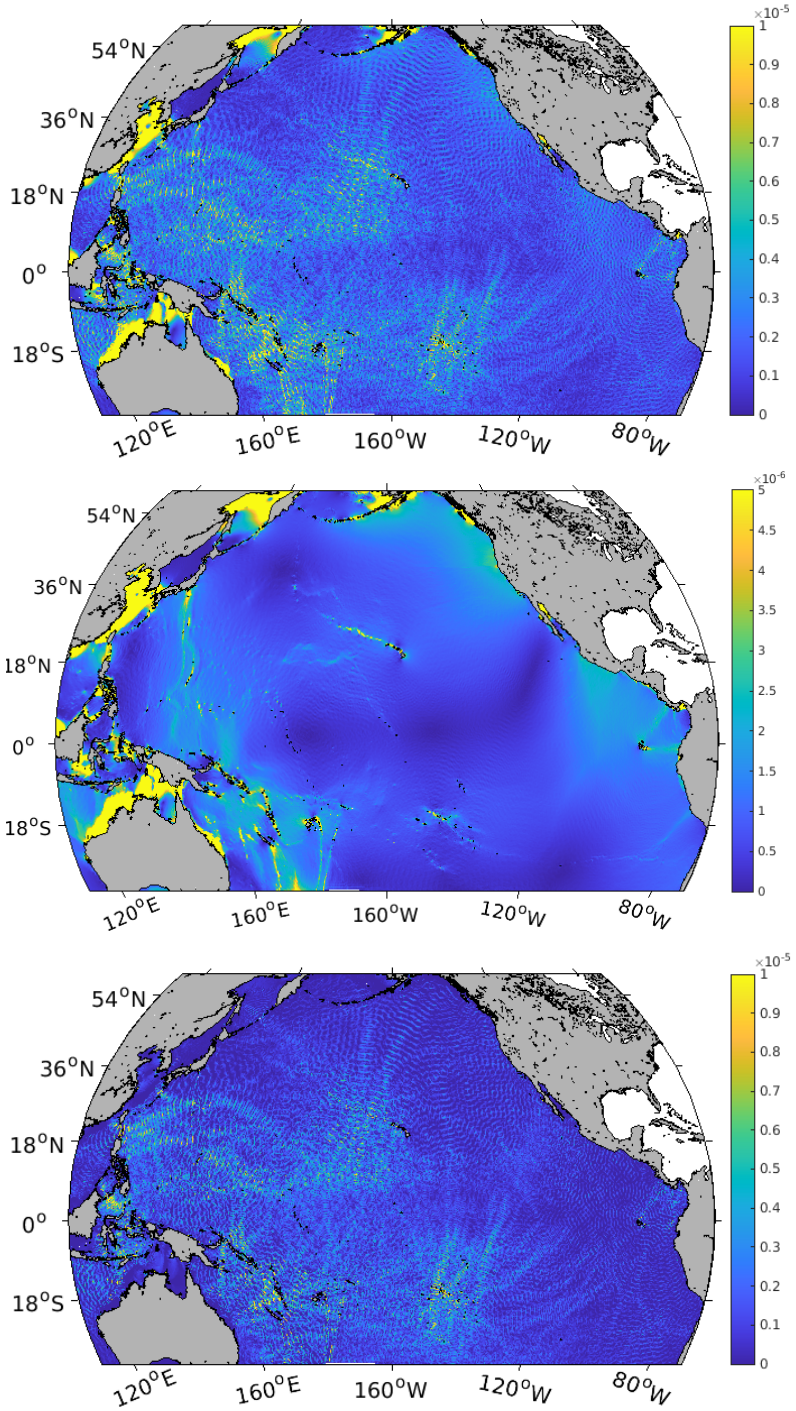

Figure 2. Cycle-averaged amplitude of (top) surface pressure-gradient $g|\nabla\zeta|$ [m s^{-2}], (middle) barotropic surface pressure-gradient magnitude $|\mathbf{P}^{bt}|$ [m s^{-2}], and (bottom) baroclinic surface pressure-gradient magnitude $|\mathbf{P}^{bc}|$ [10^{-5} m s^{-2}] for the M2 tide in the Pacific Ocean. Note the reduced colorbar range for $|\mathbf{P}^{bt}|$, which is the depth-averaged force for the barotropic mode.

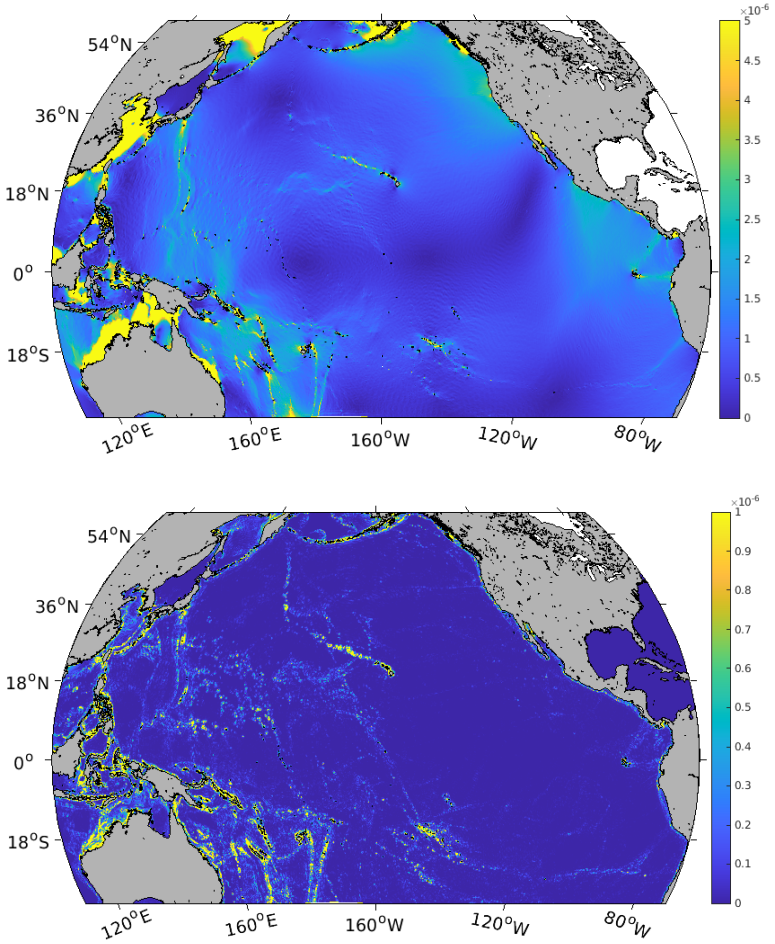

Figure 3. Decomposition of the cycle-averaged barotropic surface pressure-gradient amplitude $|\mathbf{P}^{bt}|$ [m s^{-2}] in (10) (shown as middle panel of Fig. 2) into its two parts associated with the depth-averaged pressure, $g\,|\nabla(\zeta - \widetilde{\zeta}^{bc})|$, using $\widetilde{\zeta}^{bc}$ from (15) (top), and with the interaction of the buoyancy field with the topographic gradient $|\mathbf{R}^{bc}|$ in (16) (bottom) for the M2 tide in the Pacific Ocean. Note the reduced colorbar range for $\mathbf{R}^{bc}$.

be anticipated from the linear eigenmodes at tidal frequencies, it is by no means exact due to the dynamical coupling between barotropic and baroclinic tidal components. The wide, if inhomogeneous, spatial extent of $\mathbf{P}^{bt}$ indicates that the modal dynamical coupling is not limited only to regions of barotropic-baroclinic energy conversion.

Historically, the Shallow-Water Equations have been considered as a useful approximate model for the barotropic tides (as they are for tsunamis and storm surges). In this paper we show that this view has serious limitations in its accuracy, both because Shallow-Water lacks an expression for baroclinic energy conversion and because of the sometimes strong dynamical coupling through the pressure gradient force and buoyancy field. Similarly its bottom-drag dissipation rate in deep water cannot be well represented. Going forward, more care needs to be taken in interpreting a tidal decomposition. While this is difficult in measurements because of the requirement for depth-averaging, it is feasible in 3D models such as the one used here. The best future tidal products will be made by data assimilation within such models, placing the burden of accuracy heavily on the model skill.

Appendix A Vertical modes

As an illustration of the implications of the formulas in Sec. 2.2, consider the simple situation of linear, conservative eigenmodes over a flat bottom. We will follow the notation of Kelly (2016) (*i.e.,* K16) and use rigid-lid modes with their usual diagnostic interpretation that the dynamic pressure at $z = 0$ is equal to $g\zeta$; *i.e.,* for mode n, the sea-level is

$$\zeta_n \;=\; \frac{1}{g}\, p_n(\mathbf{x},t)\, \varphi_n(0)\,, \tag{A1}$$

for $n = 0, 1, 2, \ldots$. $\varphi_n(z)$ is the separable vertical eigenfunction for pressure and horizontal velocity (*cf.,* K16, eq. (2a); *n.b.,* the notation there is ϕ_n instead of φ_n). The K16 convention on units is $U[p_n] = m^2 s^{-2}$ and $U[\varphi_n] = 1$ (*i.e.,* non-dimensional). Here $n = 0$ is the barotropic mode, and $n \geq 1$ are the baroclinic modes. (Compared to the more general free-surface modes in K16, Sec. 2, the differences are immaterial here.)

The depth-averaged modal dynamic pressure is

$$\frac{1}{H}\int_{-H}^{0} p_n \varphi_n \, dz\,. \tag{A2}$$

This equals $p_0 = g\zeta_0$ for $n = 0$ because $\varphi_0(z) = 1$. It equals zero for $n \geq 1$ because modal orthogonality implies that the depth-average of $\varphi_n(z)$ is zero (K16, eq. (7)). Thus, for the barotropic mode, $\zeta = \zeta^{bt} = p_0/g$, and $\zeta_0^{bc} = 0$.

For a flat bottom, $\widetilde{\zeta}^{bc}$ in (18) is the relevant equivalent sea level ζ^{bc} for the surface pressure gradient relation (A1) (*i.e.,* $\mathbf{R}^{bc} = 0$ here). Furthermore, the buoyancy field for mode n is

$$N^2(z)\, b_n(\mathbf{x},t)\, \Phi_n(z)\,, \tag{A3}$$

where $\Phi_n(z)$ is the vertical eigenfunction for vertical velocity (K16, eq. (2b)). $\Phi_0 = 0$ for the barotropic mode, and $d\Phi_n/dz = \varphi_n(z)$ for $n \geq 1$ to satisfy the continuity equation. The units here are $U[N] = s^{-1}$, $U[b_n] = 1$, and $U[\Phi_n] = m$. Thus,

$$\zeta_n^{bc} = \approx \frac{1}{gH}\int_{-H}^{0}\left(\int_{z'}^{0} N^2(z)\, b_n(\mathbf{x},t)\, \Phi_n(z)\, dz''\right) dz'\,. \tag{A4}$$

For $n = 0$, this is zero. For $n \geq 1$, using the boundary value problem for $\Phi(z)$ (K16, Sec. 3),

$$\zeta_n^{bc} \;\approx\; -\,\frac{b_n c_n^2}{g}\,\frac{d\Phi}{dz}(0) \;=\; \frac{p_n}{g}\,\varphi_n(0)\,, \tag{A5}$$

including the hydrostatic relation for the modal amplitude functions, $b_n = -p_n/c_n^2$, where c_n^2 is the modal eigenvalue, the square of the horizontal phase speed. Thus, for the baroclinic modes, $\zeta = \zeta_n^{bc}$, and $\zeta_n^{bt} = 0$ for $n \geq 1$. The latter implies that barotropic sea level is fully compensated by the buoyancy effect on total sea level.

Open Research Section

The ROMS code for this simulation is available at M. J. Molemaker et al. (2023), and the solution analyzed in this paper, filtered at the M2 tidal frequency is at M. J. Molemaker (2023).

Acknowledgments

We appreciate discussions with Brian Arbic in developing this paper. The research is supported by the Office of Naval Research through grant N00014-21-1-2693 and by the NSF ACCESS supercomputing centers.

References

Arbic, B. K., Alford, M. H., Ansong, J. K., Buijsman, M. C., Ciotti, R., Farrar, J. T., ... Zhao, Z. (2018). A Primer on Global Internal Tide and Internal Gravity Wave Continuum Modeling in HYCOM and MITgcm. *New Frontiers in Operational Oceanography*. (doi:10.17125/gov2018.ch13)

Barkan, R., Srinivasan, K., Yang, L., & McWilliams, J. (2021). Oceanic cross-scale energy transfers under the influence of internal waves. *Geophys. Res. Lett.*, *48*, e2021GL094376.

Capo, E., McWilliams, J., & Jagannathan, A. (2023). Topographic vorticity generation along the Spanish coast in the Alboran Sea. *J. Geophys. Res. Oceans*. (in press)

Carrere, L., Arbic, B., Dushaw, B., Egbert, G., Erofeeva, S., Lyard, F., ... Pico, N. (2021). Accuracy assessment of global internal-tide models using satellite altimetry. *Ocean Science*, *17*, 147–180.

Colosi, J., & Munk, W. (2006). Tales of the venerable honolulu tide gauge. *J. Phys. Ocean.*, *36*, 967-996.

Egbert, G., Bennett, A., & Foreman, M. (1994). TOPEX/Poseidon tides estimated using a global inverse model. *J. Geophys. Res.*, *99*, 24,821-24,852.

Egbert, G. D., & Erofeeva, S. Y. (2002). Efficient inverse modeling of barotropic ocean tides. *J. Atmos. Ocean. Tech*, *19*, 183-204. (doi:10.1175/1520-0426(2002)019<0183:EIMOBO>2.0.CO;2)

Fairall, C., Yang, M., Bariteau, L., Edson, J., Helmig, D., McGillis, W., ... Blomquist, B. (2011). Implementation of the Coupled Ocean-Atmosphere Response Experiment flux algorithm with CO2, dimethyl sulfide, and O3. *J. Geophys. Res.*, *116*, C00F09.

Hersbach, H., Bell, B., P.Berrisford, et al. (2020). The ERA5 global reanalysis. *Q. J. R. Meteor. Soc.*, *146*, 1999-2049.

Jagannathan, A., Srinivasan, K., McWilliams, J., Molemaker, M., & Stewart, A. (2021). Boundary layer mediated vorticity generation in currents over sloping topography. *J. Phys. Ocean.*, *51*, 1757-1778.

Kelly, S. (2016). The vertical mode decomposition of surface and internal tides in the presence of a free surface and arbitrary topography. *J. Phys. Ocean.*, *46*, 3777-3788.

Large, W. G., McWilliams, J. C., & Doney, S. C. (1994). Oceanic vertical mixing: A review and a model with a nonlocal boundary layer parameterization. *Rev. Geophys.*, *32*, 363-403.

Lemarié, F., Kurian, J., Shchepetkin, A. F., Molemaker, M. J., Colas, F., & McWilliams, J. C. (2012). Are there inescapable issues prohibiting the use of terrain-following coordinates in climate models? *Ocean Modelling*, *42*, 57-79.

Mellor, G. (1999). Comments on "on the utility and disutility of JEBAR". *J. Phys. Ocean.*, *29*, 2117–2118.

Molemaker, M., Damien, P., Dauhajre, D., & McWilliams, J. (2023). The Pacific echo chamber: Phase locking and patterns in the internal tide. *Nature Geosci.*. (In preparation)

Molemaker, M., Damien, P., McWilliams, J., Arbic, B., & Dollery, D. (2023). Internal tides in the Pacific: A complete energy budget. *J. Phys. Ocean.*. (In preparation)

Molemaker, M. J. (2023). Baroclinic and barotropic tidal data for the Pacific basin filtered at the M2 frequency [data set]. *Zenodo*. (https://doi.org/10.5281/zenodo.8253913)

Molemaker, M. J., Damien, P., Dollery, D., & McWilliams, J. (2023). UCLA ROMS. *Zenodo*. (https://doi.org/10.5281/zenodo.8256776)

Molemaker, M. J., McWilliams, J. C., & Dewar, W. K. (2015). Submesoscale instability and generation of mesoscale anticyclones near a separation of the California Undercurrent. *J. Phys. Ocean.*, *45*, 613-629.

Sarkisyan, A., & Ivanov, V. (1971). Joint effect of baroclinicity and bottom relief as an important factor in the dynamics of the sea currents. *Izv. Akad. Nauk SSSR, Fiz. Atmos. Okeana*, *7*, 173-188.

Savage, A., Arbic, B., Richman, J., Shriver, J., Alford, M., Buijsman, M., ... Zamudio, L. (2017). Frequency content of sea surface height variability from internal gravity waves to mesoscale eddies. *J. Geophys. Res. Oceans*, *122*, 2519–2538.

Shchepetkin, A. F., & McWilliams, J. C. (2003). A method for computing horizontal pressure-gradient force in an oceanic model with a nonaligned vertical coordinate. *J. Geophys. Res.*, *108*, 3090.

Shchepetkin, A. F., & McWilliams, J. C. (2005). The Regional Oceanic Modeling System (ROMS): A split-explicit, free-surface, topography-following-coordinate oceanic model. *Ocean Modelling*, *9*, 347-404.

Shcherbina, A. Y., D'Asaro, E. A., Lee, C. M., Klymak, J. M., Molemaker, M. J., & McWilliams, J. C. (2013). Statistics of vertical vorticity, divergence, and strain in a developed submesoscale turbulence field. *Geophys. Res. Lett.*, *40*, 4706-4711.

Song, Y. T., & Wright, D. G. (1998). A general pressure gradient formulation for ocean models. Part II: Energy, momentum, and bottom torque consistency. *Month. Weath. Rev.*, *126*, 3231-3247.

Stammer, D., Ray, R., Andersen, O., Arbic, B., Bosch, W., Carrere, L., ... Yi, Y. (2014). Accuracy assessment of global barotropic ocean tide model. *Rev. Geophys.*, *52*, 243-282.

Ubelmann, C., Carrere, L., Durand, C., Dibarboure, G., Faugere, Y., Ballarotta, M., ... Lyard, F. (2022). Simultaneous estimation of ocean mesoscale and coherent internal tide sea surface height signatures from the global altimetry record. *Ocean Science*, *18*, 469-481.

Verezemskaya, P., Barnier, B., Gulev, S., Gladyshev, S., Molines, J.-M., Gladyshev, V., et al. (2021). Assessing eddying (1/12 degree) ocean reanalysis GLORYS12 using the 14-year instrumental record from 59.5n section in the Atlantic. *J. Geophys. Res. Oceans*, *126*, e2020JC016317.